The Institute of Space and Astronautical Science
Report No. 667, March 1997

Transient Cooling of an Enclosed Fluid through Its Maximum-Density Temperature

By

Ho Sang KWAK and Kunio KUWAHARA

(February 3, 1997)

ABSTRACT: Transient cool-down process of a fluid from an initial high temperature to a target temperature in a closed container is investigated numerically. The fluid has a quadratic density-temperature relationship, and the maximum density occurring at T_m. Cooling is accomplished by abruptly lowing the sidewall temperature, and the mean temperature passes through T_m in the course of cool-down. A finite-volume method is employed to acquire numerical solutions to the full, time-dependent two-dimensional Navier-Stokes equations. In order to simulate the realistic situations under micro gravity, the Rayleigh number, Ra, encompasses the range $10^5 \leq Ra \leq 10^8$. The effects of the density inversion on the cool-down are illuminated. Based on the structures of the sidewall boundary layer, three characteristic flow regimes are identified at early time. The qualitative early-time behavior is determined by the density inversion factor. Evolutions of the global fields of flow and temperature of each flow regime are described. The analysis of time-dependent heat transfer characteristics reveals that the cool-down process is divided into several definite transient phases. The relevant time scales for the overall cool-down process are estimated. The specific effects of the Rayleigh number, density inversion factor, and the aspect ratio of the container on each evolutionary stage are elaborated.

1. INTRODUCTION

In liquid storage tanks equipped in space facilities, it is often required that the contained fluid should be maintained at a low temperature. Cool-down of a liquid from the initial-state high temperature to a target temperature is a crucial mission in this system. Cooling is accomplished by adopting cooling elements around the tanks. Under terrestrial condition, the Rayleigh number, Ra, which is a principle control parameter of these problems, is very large, i.e., $Ra = 10^{10} \sim 10^{15}$. Transient cool-down process is governed by fully turbulent convection. Even under micro-gravity condition ($g \sim 10^{-5} g_o$, g_o is the terrestrial gravity), Ra is still large, $Ra \gg 1$, i.e., the buoyancy effects are substantial. Cool-down is driven by natural convection rather than by conduction. A key element is to predict the time scale for the fluid to reach a desired temperature level. These are based upon a proper understanding of the time-dependent structures of flow and temperature fields.

Another concern of the present study is the effects of density inversion in the course of cool-down. Transient buoyant convection of an initially-isothermal fluid in an enclosure, in response to the changes in thermal boundary conditions, has been widely studied. Discussions have been centered on the evolutions of convective flow pattern and temperature field, and to the relevant scales of time, velocity and boundary layer thickness. Comprehensive reviews on this subject were given by Ostrach [*1*] and Hyun [*2*]. The great majority of previous studies have been performed under the Boussinesq fluid approximation, which stipulates a linear relationship between density and tempera-

ture. However, for water and certain liquids, density can not be described by a monotonic linear function of temperature near the melting point (see, e.g., [3]). Instead, density ρ reaches its maximum at a specific temperature T_m, and ρ decreases when temperature deviates from T_m in both directions. The best known example is water which has maximum density at $T_m = 3.98$℃ and many beverages have a similar property. This nonlinear behavior, termed the density inversion, brings forth a major dynamic ingredient to natural convection.

Recently, buoyant convection of an enclosed fluid with density inversion has been studied by numerical computations and laboratory experiments [*4-16*]. These works revealed the prominent impacts of the density inversion in various flow configurations. Most of these studies deal with primarily steady-state situations [*4-10*]. A literature survey discloses that comparatively scanty attention has been given to transient natural convection with density inversion.

Robillard and Vasseur [*11*] investigated convective cooling of water near 4℃ in a rectangular cavity with a constant cooling rate applied on all boundaries. Numerical and experimental studies on the transient natural convection of water in a sidewall-heated cavity were recently conducted by Braga and Viskanta [*12*] and McDonough and Faghri [*13*]. In the initial state, motionless and isothermal water at a high temperature $T_i (\geq T_m)$ filled the rectangular cavity. The temperature of one sidewall was abruptly lowered and kept at $T_w = 0$℃, while the opposing wall temperature was maintained at the initial value $T_h = T_i$. Tong and Koster [*14*] numerically investigated a similar problem using different initial conditions, i.e., $T_i = T_m$. Numerical solutions demonstrated good agreement with the experimental results, which illustrated the general influences of density inversion on the transient flow and temperature fields and heat transfer characteristics.

Systematic studies of cool-down (or heat-up) of the entire body of an initially-isothermal liquid with density inversion to a desired temperature have been scarce. Vasseur and Robillard [*15*] and Robillard and Vasseur [*16*] numerically investigated the transient natural convection of water in a rectangular cavity, with varying aspect ratios and initial water temperatures in the range $4℃ \leq T_i \leq 10℃$. Temperatures at all solid boundary walls were abruptly changed to 0℃. Time-dependent evolutions of the subsequent flow and temperature fields were portrayed. However, their results were restricted to the range of relatively small Rayleigh numbers, 2.9×10^3 to 8×10^4. Therefore, the convection effects were not pronounced; consequently, the time-dependent variations of the numerically-acquired Nusselt number did not deviate much from the pure conduction solution. In addition, due to the limited coverage of the relevant parameters, the effects of the Rayleigh number and of the initial temperature (the density inversion factor) on the global cool-down process were not elucidated.

In this study, comprehensive and detailed numerical simulations are carried out to describe the cool-down of a liquid contained in a vertical cylinder through its maximum-density temperature; the entire body of an enclosed fluid of initial temperature $T_i (\geq T_m)$ is cooled by altering the sidewall temperature abruptly to $T_w (< T_m)$. The present calculations cover a much extended range of values of the Rayleigh number, aspect ratio and density inversion factor. The objective is to gain a thorough basic understanding of the underlying physical phenomenon in the convective cool-down process encompassing the maximum-density temperature. The impetus of this paper is to depict dominant transient flow and temperature fields and the associated cooling characteristics of earlier stages of cool-down. Emphasis will be given to the specific impacts of density inversion on the transient cooling process. Special concern will be devoted to depicting the distinctive transient phases in the course of cool-down. Scalings will be provided to characterize each transient stage and the influences of the principle parameters on the overall cool-down time scales will be scrutinized.

2. MATHEMATICAL FORMULATION

Consider a vertically-mounted cylinder of radius R and vertical height H, which is completely

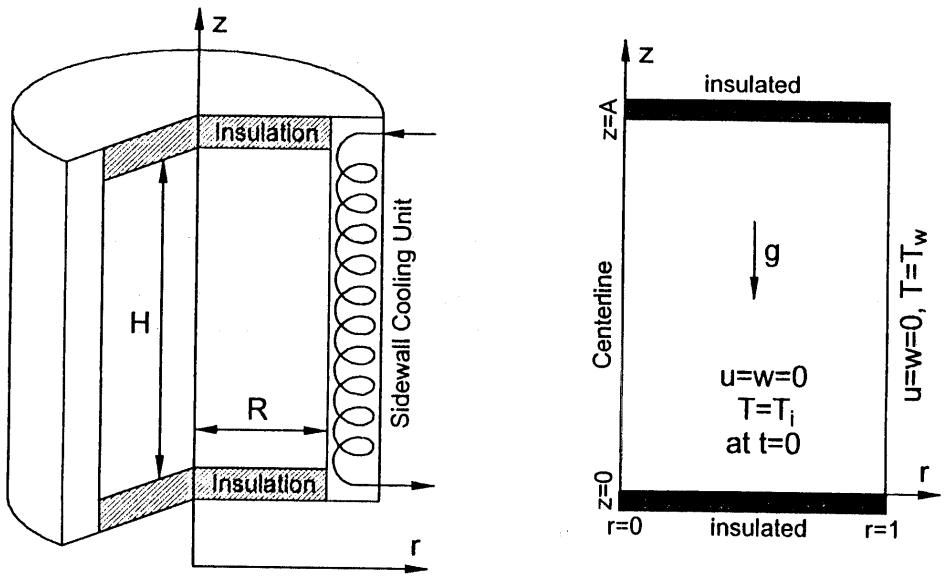

(a) Cool-down System by Sidewall Cooling (b) Numerical Model

Fig. 1. Schematic diagram of the flow configuration.

filled with a liquid of kinematic viscosity ν, thermal diffusivity κ. The vertical axis of the cylinder is antiparallel to the gravity. Maximum density of the fluid, ρ_m, occurs at the temperature $T=T_m$. The fluid is initially at rest and isothermal at temperature $T_i(\geq T_m)$. At $t=0$, the whole vertical sidewall is abruptly cooled to temperature $T_w(<T_m)$. The horizontal endwalls are thermally insulated. Fig. 1 shows a schema of the flow configuration and coordinate system. It is assumed that the fluid is Newtonian and incompressible, and all the fluid properties are constant except for the density in the buoyancy term. The density ρ is assumed to obey a quadratic density-temperature relationship in the vicinity of the maximum-density temperature T_m [*17*]:

$$\frac{\rho}{\rho_m}=1.0-\beta\,(T-T_m)^2, \tag{1}$$

where β is the volumetric expansion coefficient for a density-inversion fluid.

For comparison, the conventional Boussinesq fluid approximation states a linear density-temperature relationship:

$$\frac{\rho}{\rho_r}=1.0-\alpha\,(T-T_r), \tag{2}$$

where ρ_r and T_r indicate reference quantities and α is thermometric expansion coefficient for a Boussinesq fluid.

The flow is governed by the time-dependent Navier-Stokes equations, which, in nondimensional form, are expressed as

$$\frac{\partial u}{\partial t}+\frac{1}{r}\frac{\partial}{\partial r}(ru^2)+\frac{\partial}{\partial z}(wu)=-\frac{\partial p}{\partial r}+\left(\frac{Pr}{Ra}\right)^{1/2}\left(\nabla^2 u-\frac{u}{r^2}\right), \tag{3}$$

$$\frac{\partial w}{\partial t}+\frac{1}{r}\frac{\partial}{\partial r}(ruw)+\frac{\partial}{\partial z}(w^2)=-\frac{\partial p}{\partial z}+\theta^2+\left(\frac{Pr}{Ra}\right)^{1/2}\nabla^2 w, \tag{4}$$

$$\frac{\partial\theta}{\partial t}+\frac{1}{r}\frac{\partial}{\partial r}(ru\theta)+\frac{\partial}{\partial z}(w\theta)=\left(\frac{1}{RaPr}\right)^{1/2}\nabla^2\theta, \tag{5}$$

$$\frac{1}{r}\frac{\partial(ru)}{\partial r}+\frac{\partial w}{\partial z}=0, \tag{6}$$

where $\nabla^2=\frac{1}{r}\frac{\partial}{\partial r}r\frac{\partial}{\partial r}+\frac{\partial^2}{\partial z^2}$. In the above, standard notation is employed, i.e., p is the pressure, θ the temperature, t the time, (r, z) the radial and vertical coordinates, and (u, ν) the velocity components corresponding respectively to (r, z) directions. Non-dimensionalization was effectuated in the following fashion:

$$t=t^*(RaPr)^{1/2}\frac{\kappa}{R^2}, \tag{7}$$

$$(u, w)=(u^*, w^*)\ (RaPr)^{-1/2}\frac{R}{\kappa}, \tag{8}$$

$$(r, z)=(r^*, z^*)/R, \tag{9}$$

$$\vartheta=\frac{T-T_m}{T_m-T_w}, \tag{10}$$

$$P=\frac{(p^*+\rho gz^*)R^2}{\rho\kappa^2RaPr}, \tag{11}$$

where * denotes dimensional quantities and g is the gravitational acceleration.

The relevant non-dimensional parameters are

$$Ra=\frac{(\rho_m-\rho_w)gR^3}{\rho_m\nu\kappa}, \quad \text{the Rayleigh number;} \tag{12}$$

$$Pr=\nu/\kappa, \quad \text{the Prandtl number;} \tag{13}$$

$$A=H/R, \quad \text{the aspect ratio of the cylinder;} \tag{14}$$

Note that, as shown in equation (12), the Rayleigh number is defined by using the difference between the maximum density and the density at the cold sidewall. This definition of Ra is similar to that of the cold-side Ra adopted by Lankford and Bejan et al. [*6*]. A slightly different form of Ra was selected in Refs. [*12, 13, 15*], in which the density difference $\Delta\rho\equiv\rho_m-\bar{\rho}$, $\bar{\rho}$ denoting the density at the mean temperature $(T_i+T_w)/2$, was employed.

In line with the problem description, the initial and boundary conditions are

$$u=w=0 \text{ and } \theta=\gamma, \text{ for } t<0, \tag{15}$$

where

$$\gamma=(T_i-T_m)/(T_m-T_w), \tag{16}$$

and for $t\geq 0$

$$u=w=0 \text{ and } \theta=-1 \text{ at } r=1; \tag{17}$$

$$u=\frac{\partial w}{\partial r}=\frac{\partial \theta}{\partial r}=0, \text{ at } r=0; \tag{18}$$

$$u=w=\frac{\partial \theta}{\partial z}=0, \text{ at } z=0 \text{ and } z=A. \tag{19}$$

Clearly, γ in equation (16) indicates the level of the initial-state temperature T_i, relative to T_m and T_w; γ will be termed the density inversion factor.

3. NUMERICAL MODEL

The system of equations (3)-(6) was solved numerically by employing a finite-volume procedure based on the SIMPLER algorithm [*18*]. The governing equations were discretized on a staggered grid. Spatial differencing schemes of the second-order accuracy were adopted for the equation terms. A central differencing was used for the diffusion terms, and a recent version of the QUICK scheme [*19*] was utilized for the nonlinear convective terms. All of the boundary conditions were treated by using second-order differencings. Time integration was accomplished by using an iterative Eulerian implicit method of first order accuracy in time. The resulting accuracy of the present numerical method is $O(\Delta x, \Delta t^2)$, where Δx is the grid spacing and Δt the time step used in calculations. Convergence of the solutions was declared at each time step when the maximum relative change between two consecutive iteration levels falls below 10^{-4} for u, w and θ. A parallel checking was performed to ensure that mass continuity in every computational control volume should be satisfied within a relative error 10^{-8}.

Verification of the present numerical model was achieved by repeating a multitude of calculations of the previous results [*12-15*]. Fig. 2 illustrates the reliability and accuracy of the present numerical model. The experiment No. 1 ($T_i=T_h=8$℃, $T_w=0$℃, $Pr=11.82$) of Braga and Viskanta [*12*] was reproduced and the results at two time instants were compared with their numerical and experimental results. For this test, a strectched grid network of 62×62 nodes was used and Δt was 1 second. The flow patterns and temperature fields are generally similar to those of numerical results of Braga and Viskanta (see Figs. 2-3 in [*12*]). The difference can be found in the size of the circulating cell in the lower left corner. The present numerical model produced a bigger cell, which is in closer agreement with the visualized flow patterns (Fig. 4 in [*12*]). Comparisons were also made of the horizontal temperature profiles at three representative heights (Fig. 5 in [*12*]). Fig. 2(c) reveals that the present numerical model gives a better prediction of the experimental data than that of Braga and Viskanta [*12*]. Thease results illustrate the reliability of the present model. The improved agreement with experimental results can be attributable to the fact that the present numerical method adopted higher-order spacial differencing schemes than that of Braga and Viskanta [*12*]. Additional runs were repeated with different grids and time steps. For the temperature field at 15min (at 30min), the maximum difference between 62×62 and 82×82 nodes was 4.9% (10.4%) and the maximum difference between 62×62 and 102×102 nodes was 5.8% (15.3%). The large differences were monitored only near the border between the two counter-rotating cells across which the temperature varies sharply. In the other regions, the differences at 15 minute (30 minute) were less than 1% (2%). The solutions were shown to be almost insensitive to Δt if Δt is small enough to resolve the boundary layer formation.

For the present problem, numerical computations were conducted for selected sets of (Ra, A) by varying γ in the range $0\leq\gamma\leq3.0$. The parameters were chosen to simulate realistic problems under micro-gravity condition; the selected values of Ra and A were $Ra=10^5$, 10^6 and 10^7, and $A=1.0$, 2.0, 5.0, 10.0. The resulting Rayleigh number based on the height of the cylinder, Ra_H, encompassed the range of $10^5\leq Ra_H\leq10^8$. The Prandtl number, Pr, was set $Pr=11.573$, which is the typical value for

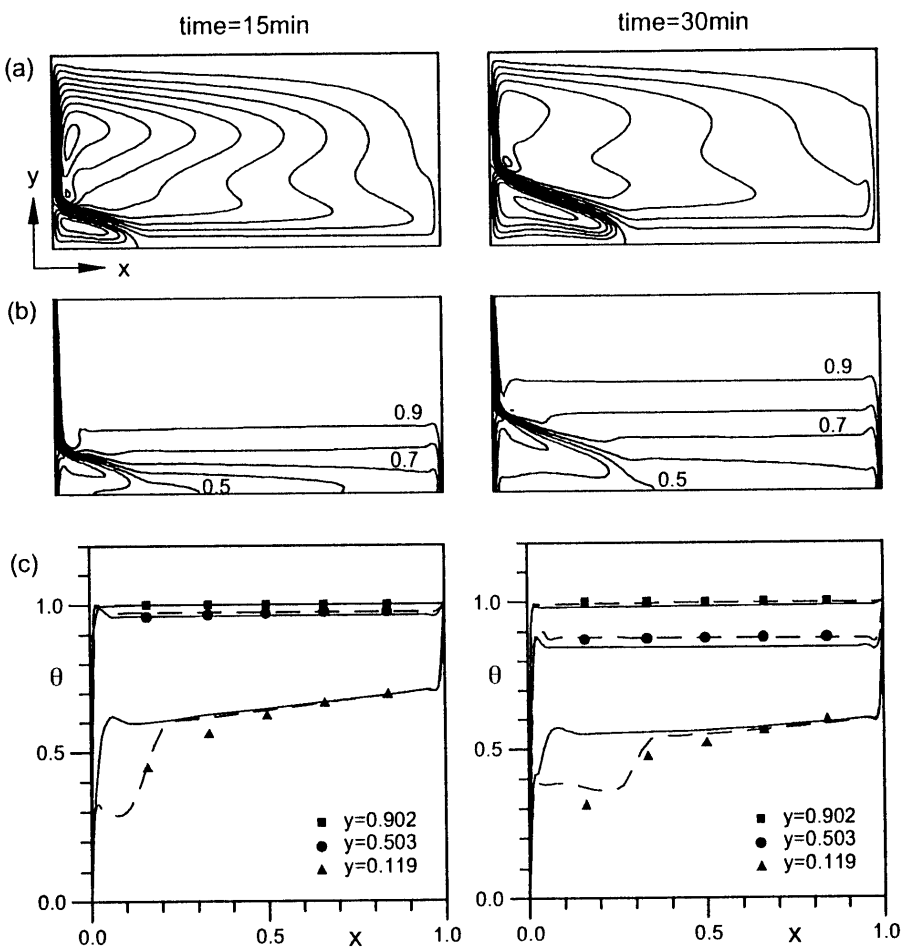

Fig. 2. Results of a verification test of the present numerical method for Experiment No. 1 of Braga and Viskanta [*12*]. The time instants are 15 minute for left column and 30 minute for right column. (a) Predicted streamlines, (b) predicted isotherms, (c) horizontal profiles of temperature at three different height. In Fig. 2(c), the solid lines and symbols represent the numerical and experimental results of Braga and Viskanta [*12*], respectively and the present numerical results are shown by broken lines.

Table 1. Computed sets of (Ra, A), and grid points and time steps used for calculations.

Ra	A	Number of grid	time step, Δt
10^5	1.0	52×52	0.01
10^6	1.0	62×62	0.01
10^7	1.0	72×72	0.01
10^5	2.0	62×72	0.01
10^5	5.0	72×102	0.005
10^5	10.0	82×122	0.005 for $\gamma\leq1.0$ 0.002 for $\gamma>1.0$

water near 3.98°C. Depending on the value of Ra and A, different grid meshes and time step were used. To resolve thin boundary layers adjacent to the solid walls, grid stretching was implemented such that at least 5 grid points were located in the boundary layer. The computed cases, grids and time steps used in the present calculations are listed in Table 1.

4. EARLY-TIME FLOW CHARACTERISTICS

Before proceeding further, it is helpful to have a brief overview of the flow structure adjacent to the sidewall at very early times. It is noted that $Ra/Pr^4 \gg 1$ for all the present runs. Based on the scaling argument of Patterson & Imberger [*20*], the flow regime in the early stage is of the boundary-layer type. In response to the impulsive change in the sidewall temperature, the thermal boundary layer forms on the sidewall, in which vertical flow is induced by buoyancy force. This layer grows until the heat conducted out to the sidewall balances that convected in by the vertical currents. Since $Pr > 1$, momentum is diffused into the core outside the thickness of thermal boundary layer. This generates a secondary viscous layer, which is governed by the inertia-viscous balance. This assertion is valid in depicting the general early-time behavior of cool-down. However, in comparison with the

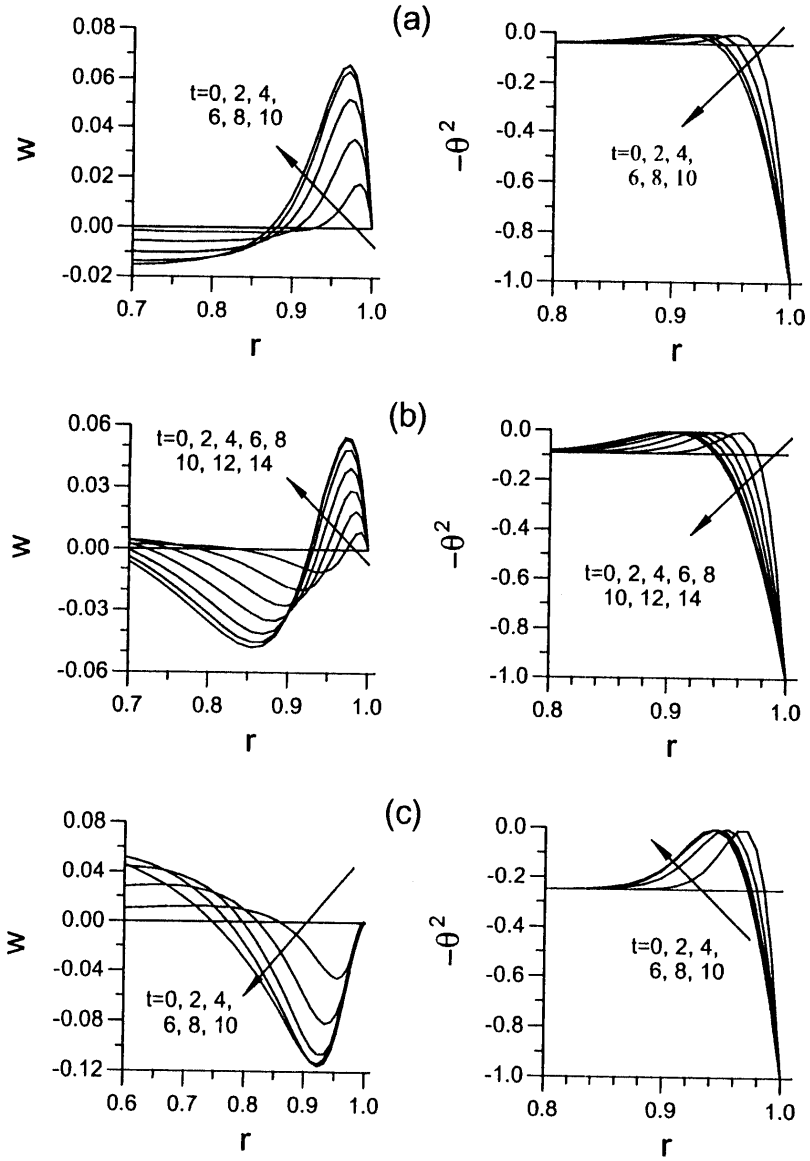

Fig. 3. Early time evolutions of vertical velocity (left column) and density (right column) near the sidewall at $z=0.5$. $Ra=10^6$, $A=1.0$. (a) $\gamma=0.2$; (b) $\gamma=0.3$; (c) $\gamma=0.5$.

Boussinesq fluid, the buoyancy-induced flow of a fluid with density inversion presents a more complicated picture.

Fig. 3 exemplifies the structures of vertical boundary layer, which depict the early time evolutions of vertical velocity and density near the sidewall at the vertical mid-depth plane ($z=A/2$). The influence of the density inversion in determining the buoyancy force is schematically illustrated. For $\gamma>0$, there exists a buoyancy force reversal inside the thermal boundary layer; the sign of the buoyancy force is positive (upward) in the wall-side of the boundary layer while it is negative (downward) in the core-side (see, e.g., [*21, 22*]). Owing to this character, three flow patterns, depending on the value of γ, can be identified at early times in the thermal boundary layer.

When γ is small (see Fig. 3(a)), the positive buoyancy force prevails in the bulk of the vertical thermal boundary layer. Only in a narrow zone of the layer, the negative buoyancy exists. However, this negative buoyancy is outweighed by viscous shear force, which is locally effective in such a thin area between the dominant upward motion and the solid wall. Consequently, the resulting boundary layer flow is predominantly upward, which is referred to as flow regime I. On the other hand, for large γ (see Fig. 3(c)), a situation opposite to the cases of small γ develops. The buoyancy force is mostly negative in the vertical thermal boundary layer. The positive buoyancy force is restricted in a very narrow region adjacent to the sidewall. Accordingly, the flow in the vertical thermal boundary layer is predominantly downward, which is referred to as flow regime III. The intermediate pattern, flow regime II, is illustrated in Fig. 3(b). For a moderate value of γ, a flow reversal, associated with the

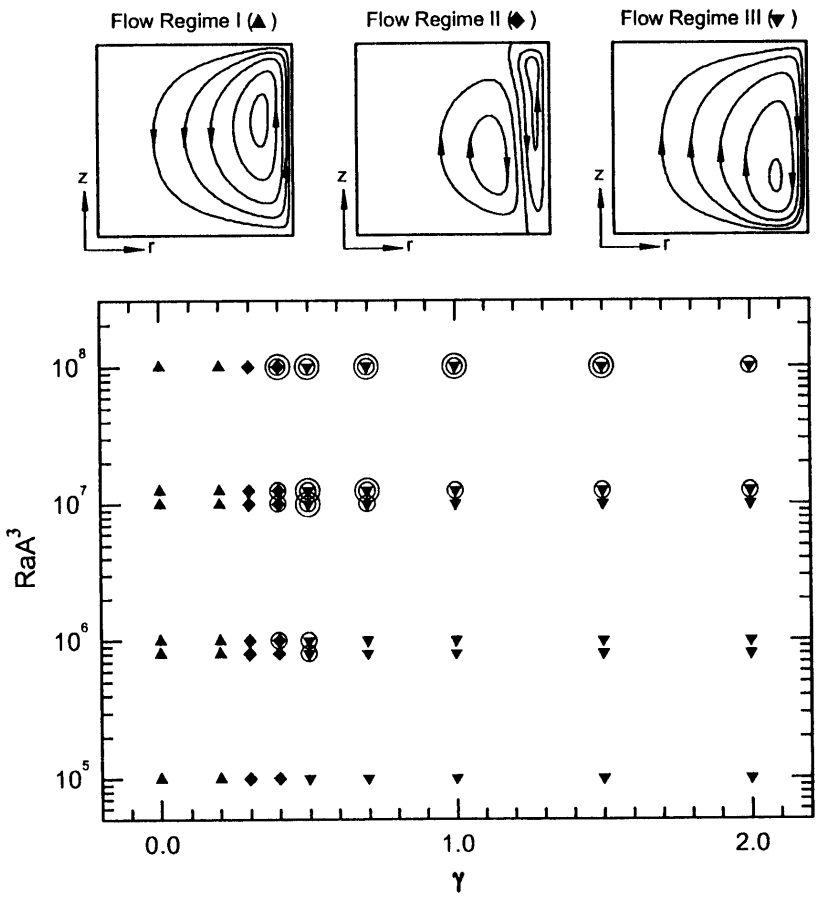

Fig. 4. Summary of the results in the γ-Ra domain. In the figure, ▲ represents flow regime I; ◆, flow regime II; ▼, flow regime III. A single circle represents the cases in which a weak secondary boundary layer wave forms. The double circles indicate the cases in which more than three boundary layer waves are developed.

buoyancy force reversal, exists; both the upward and downward motions are present in the vertical thermal boundary layer. This is the case when the magnitudes of positive and negative buoyancy forces are comparable. It is noteworthy that the velocity profiles of flow regimes II and III resemble those of the lower and upper branch similarity solutions for the case of an infinite vertical wall with density inversion [*21, 22*].

The results of the present runs are summarized in Fig. 4. The essential qualitative character of flow in the early stage of cool-down can be classified into the above-described three categories. Fig. 4 indicates that the influences of Ra and A in determining the flow regime are generally meager. The qualitative flow characteristics at early times of the cool-down process are determined mainly by a single parameter γ. In the present study, only discrete points in the parameter space were covered. Therefore, it posed difficulties in evaluating the exact values of γ at which demarcations between two flow regimes are located. Obviously, flow regimes I and III are seen for small and large values of γ, respectively, and flow regime II occurs only in a narrow range of γ.

5. DESCRIPTION OF THE OVERALL TRANSIENT COOL-DOWN

Exemplary plots showing the transient flow patterns and temperature fields of flow regime I are illustrated in Fig. 5 for $Ra=10^6$, $A=1.0$, and $\gamma=0.0$. For this specific case with no density inversion, the overall cool-down process is qualitatively similar to that for a Boussinesq fluid with a negative value of α in equation (2). At small times, the thermal boundary layer forms on the sidewall and the upward flow in this layer drives the counter-clockwise (CCW) circulations. The thermal boundary layer forms on the sidewall and it grows to a thickness $\delta_T \sim O(Ra^{-1/4}Pr^{1/2}A^{1/4})$ in time $t \sim O(Pr^{1/2}A^{1/2})$ [*2, 20*]. The heat transfer rate at the sidewall is estimated as

$$\frac{\partial \theta}{\partial r}\Big|_{r=1} \sim \frac{\theta}{\delta_T}. \tag{20}$$

As the sidewall boundary layer is fully developed, the upwelling currents via the sidewall boundary layer produce a viscous intrusion layer, which propagates in the horizontal direction near the upper endwall, as displayed in Fig. 5(b). The front of the cold fluid parcels moves downward in the interior core after the horizontal intrusion layer reaches the central axis of the cylinder. Following the front movement, a stable density stratification is established in the interior core as shown in Fig. 5(c). The CCW circulation cell fills the full cylinder and the interior stratification is established with the fluid of $\theta<0$. According to the previous scaling argument [*2, 20*], this process takes a convective time scale, $t \sim O(Ra^{1/4}Pr^{1/2}A^{1/4})$. In this transient phase, the structure of the thermal boundary layer is largely unchanged. Consequently, the heat transfer rate in this phase remains almost constant.

Afterwards, convective cooling in the interior progresses, and the mean temperature (density) of the interior fluid decreases. The circulations weaken with time and cool-down in this stage slows down. Finally, the flow undergoes a slow diffusively-controlled approach toward the stationary and isothermal steady state.

Fig. 6 typifies transient flow and temperature fields of flow regime II for $Ra=10^6$, $A=1.0$, and $\gamma=0.3$. At very early times, the thermal boundary layer forms on the sidewall. Fig. 6(a) demonstrates the presence of flow reversal in the vertical thermal boundary layer. Both the upward and downward flows are developed in the wall-side and core-side regions of the thermal boundary layer, respectively. These produce an isolated CCW circulation cell near the sidewall. Noting $Pr>1$, the downward momentum (velocity) is diffused into the viscous layer outside the thermal boundary layer, which creates a clockwise (CW) circulation cell in the interior. Consequently, the flow field is characterized by a bi-cellular structure, which consists of two counter-rotating cells.

Similarly to the case of $\gamma=0$, the horizontal propagation of intrusion layer is visible in Fig. 6(b). However, following the intrusion, the region occupied by the isolated CCW cell is expanded in the

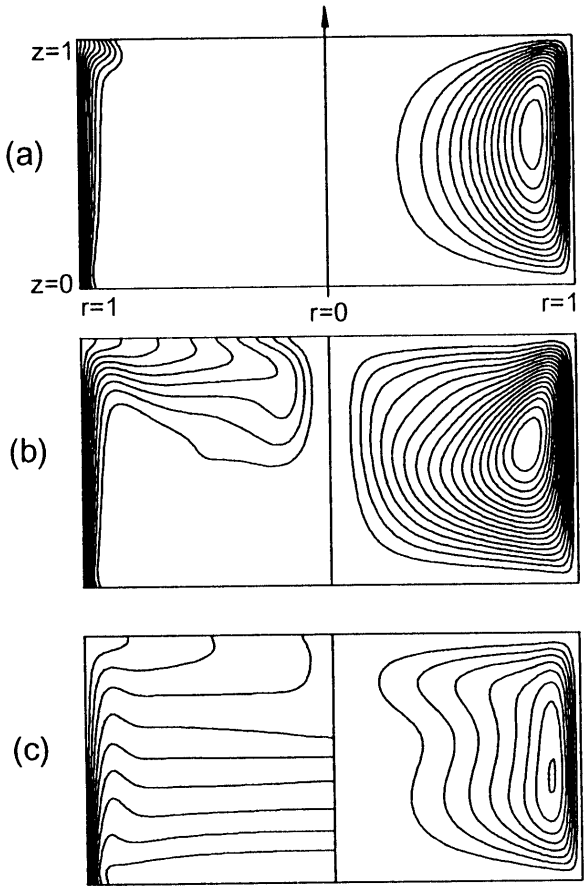

Fig. 5. Sequential plots showing isotherms (left column) and stream functions (right column). $Ra=10^6$, $A=1.0$, and $\gamma=0.0$. The time instants are (a) $t=5$; (b) $t=20$; (c) $t=60$. The contour increments are $\Delta\psi=0.0005$ and $\Delta\theta=0.1$.

neighborhood of the upper horizontal endwall. The border between the CW and CCW cells approximately coincides with the line of density maximum ($\theta=0$), as was reported in [*12-14*]. The front of the cold fluid parcels moves downward in the interior as the horizontal intrusion is being accomplished. The CCW circulations fill the full cylinder and the subsequent transient characteristics are similar to those in the final stage of cool-down described for $\gamma=0$.

The transient response of flow regime III is exemplified in Fig. 7, for $Ra=10^6$, $A=1.0$, and $\gamma=1.0$. As in the afore-described regimes, the vertical thermal boundary layer forms at early times, as shown in Fig. 7(a). The flow in the vertical thermal boundary layer is entirely downward. Accordingly, the full cylinder has the CW circulations only, and the horizontal intrusion is seen in the lower part of the cylinder. It is noticeable in Fig. 7(b) that two CCW circulation cells appear; one in the central part and the other near the lower sidewall corner. The former is due to the local baroclinicity reversal (change in the sign of $\partial\rho/\partial r$) in the central region. This cell is maintained in a short period, and its impact on the overall cool-down process is minor.

It is useful to monitor the evolution of the latter CCW circulation cell. The horizontal intrusion delivers cold fluid parcels to the lower part of the cylinder. The maximum density line ($\theta=0$) moves further toward the interior side, which produces a different environment for the fluid in the lower corner region. In the lower corner region, θ becomes negative and ρ decreases monotonically toward the sidewall. Consequently, the positive buoyancy force is created in this region. This, in turn, induces upward velocity near the sidewall, which generates a new CCW circulation cell isolated in the lower corner region.

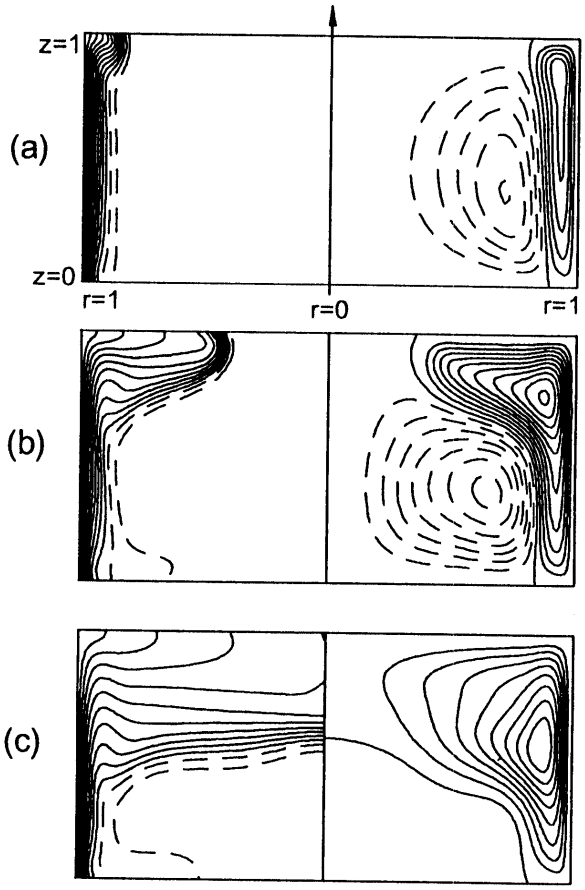

Fig. 6. Same as in Fig. 5, except for $\gamma=0.3$. (a) $t=10$; (b) $t=30$; (c) $t=60$. Isotherms of positive θ, and the contours for negative ϕ (CW circulation) are shown by broken lines.

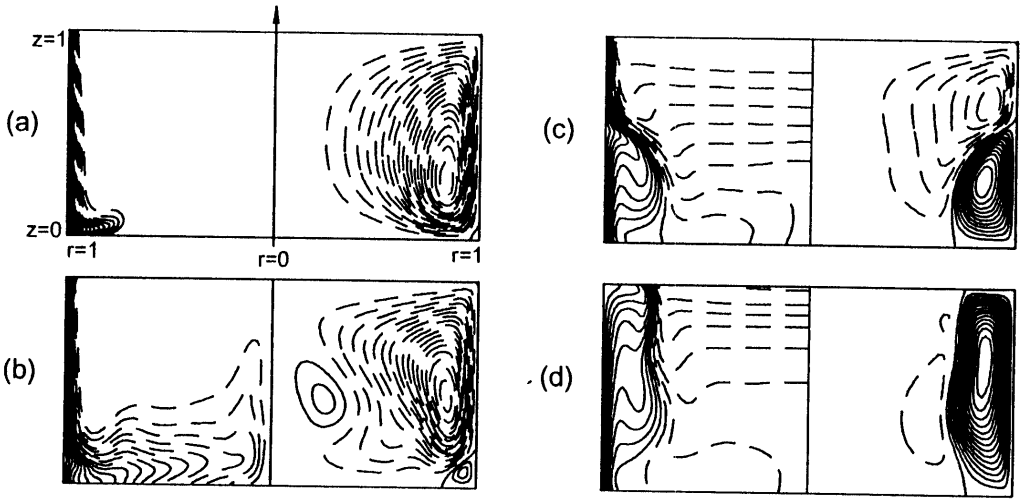

Fig. 7. Same as in Fig. 6, except for $\gamma=1.0$. (a) $t=3$; (b) $t=20$; (c) $t=30$; (d) $t=60$. $\Delta\phi=0.0005$ for positive ϕ and $\Delta\phi=0.001$ for negative ϕ.

Here, it is important to describe the roles of the CW and CCW circulations. The CW circulations provide convective cooling in the interior by delivering cold fluid parcels which was cooled at the sidewall. Due to the CW circulations, the front of cold fluid parcels propagates upward. Following the front, stable density stratification is established in the interior. With the progress of the core stratification, the CW circulations weaken and they vanish at large times. Heat transfer at the sidewall in the region of the CCW circulation cell (below the separation point) gives rise to cooling for the fluid in this isolated region. This causes the isolated CCW circulation cell to grow with time. Since the stable stratification in the interior blocks the horizontal expansion, this CCW circulation cell grows mainly in the vertical direction along the sidewall as shown in Figs. 7(b-d). This transient character, termed the sidewall boundary layer restructuring, is a phenomenon unique to flow regime III.

The boundary layer restructuring implies that there exists a separation point on the sidewall across which the flow changes its direction. The boundary-layer flows below and above this point have similar qualitative structures to those of the lower and upper branch similarity solutions for the boundary layer on an infinite vertical wall with density inversion [*4, 5*]. The thermal boundary layer thickness above the separation point is much smaller than that below the separation point. Consequently, the heat transfer rate decreases with the advance of boundary layer restructuring.

As the sidewall boundary layer restructuring is fully achieved, a second horizontal intrusion appears in the upper part of the cylinder. The transient process afterwards is akin to that of flow regime II.

The flow restructuring in the cool-down of an enclosed fluid with density inversion was reported by Vasseur and Robillard [*15*]. They presented the half-domain numerical solutions by assuming the symmetry about the vertical center line. Fig. 2 in [*15*] showed the presence of three transient stages, which depicted the results of the specific case for $\gamma=1.0$ (this belongs to the flow regime III of the present paper). At the beginning of cooling process, a CW circulation cell is induced in the right half cavity. In the next stage, a CCW circulation cell is created from the lower right corner region, and it grows upward to push the original CW circulation cell. Finally, only the newly-developed CCW circulation fills the right half cavity. However, the transient restructuring in [*15*] was not restricted in the region adjacent to the sidewall; the newly-developed CCW circulation cell occupies the full lower part of the cavity, spanning horizontally from the interior to the sidewall. As a result, the flow pattern in the second stage displays two counter-rotating circulation cells which are vertically stacked. All the results in [*15*] illustrated the same characteristics. This discrepancy can be attributed to the difference in the thermal boundary condition; the horizontal walls of the cavity considered by Vasseur and Robillard [*15*] are a perfectly conducting wall of $T=T_w$, while the upper and lower endwalls of the present cylinder are thermally insulated. Due to the constant-temperature condition at the horizontal walls, the line of the maximum density lied in the horizontal direction. Along this line, the newly-developed CCW circulation could grow in the horizontal direction.

The transient phenomenon similar to the boundary layer restructuring was also explored in unsteady natural convection of a fluid near its density maximum in a sidewall-heated cavity [*12-14*]. The transient flow patterns for the cases with a large density inversion reveal a pair of counter-rotating circulation cells. Near the lower corner of the cold wall, a circulation cell is seen which rotates in the opposite direction to the dominant circulation which occupies most of the cavity. It is conspicuous in Fig. 3 of [*13*] that this corner cell grows upward along the sidewall. Owing to the constraint in the problem setup, this cell stopped growing at a certain vertical level. The full boundary layer restructuring depicted in the present cool-down problem was not discussed explicitly.

6. BOUNDARY LAYER WAVES

It is of value to point out one finding of interest. Fig. 8 shows the results at a high Ra ($Ra=10^7$), with $\gamma=0.5$, and $A=1.0$. The general features of boundary layer restructuring process are similar to

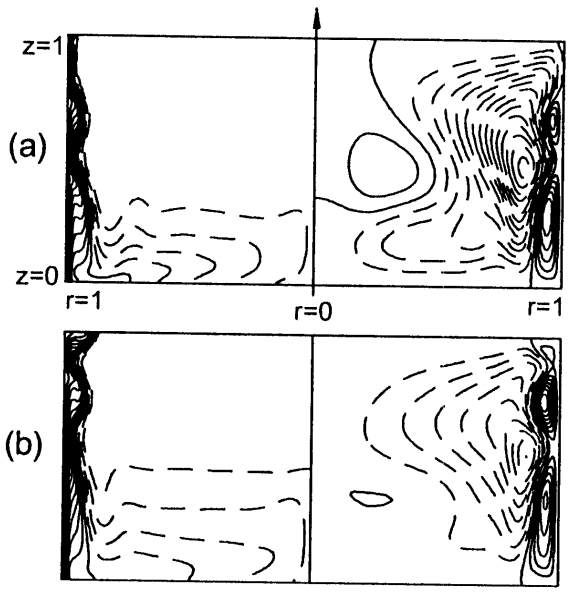

Fig. 8. Same as in Fig. 6, except for $\gamma=0.5$, $Ra=10^7$. (a) $t=25$; (b) $t=40$.

that in Fig. 7. However, it is clearly visible that the wave-like flow patterns form in the boundary layer below the separation point. There exist two centers of the CCW circulations. Following the primary mode, secondary and higher-mode waves are discernible and they move in the upward direction with time.

These transient flow characteristics are also monitored at a lower Ra with a large aspect ratio. Fig. 9 exemplifies the boundary layer restructuring process for $Ra=10^5$, $A=10.0$, and $\gamma=0.5$. Initially, a CCW cell appears in the lower corner region and it moves upward. However, the boundary layer below the separation point becomes unstable, thus, generates subsidiary modes. In Fig. 9(c), three waves traveling along the sidewall are seen. The flow exhibits several CCW cells and CW cells, which are arranged in the vertical direction. After the primary mode of the boundary restructuring reaches the upper endwall, the cold parcels propagate downward in the interior core region. The developed waves travel upward and disappear eventually as the front of cold fluid parcels moves downward in the interior core.

The above-described boundary layer waves were previously ascertained in other flow configurations, e.g., natural convection of a Boussinesq fluid in the sidewall-heated cavity [*23, 24*]. For a very large Ra with $A=O(1)$ [*23*], or a moderately large Ra with a large A [*24*], boundary layer waves were reported to develop in the sidewall boundary layer. One assertion is that these waves may be responsible for bringing permanent unsteadiness and, thus, providing origins of turbulence.

The present results concerning the existence of boundary layer waves are also summarized in Fig. 4. It is obvious that the boundary layer waves are captured when Ra and A are large, namely, the Rayleigh number based on the vertical height of the cylinder, $Ra_H(\equiv RaA^3)$, is sufficiently large. At a relatively small Ra_H (indicated with a single circle in Fig. 4), only a weak secondary wave forms but it soon decays due to the pronounced viscous and thermal diffusions. At a larger Ra_H, the generation of boundary layer waves becomes more active, and several succeeding modes are created although they disappear eventually with the progress of cool-down. Here, it is worth pointing out that, in the present cool-down problems, the boundary layer waves are developed at a much smaller Ra_H than for a Boussinesq fluid. In a sidewall-heated cavity with $A=1$, they are seen for $Ra\sim10^9$ [*23*]. In particular, as shown in Fig. 4, the boundary layer waves are developed at much smaller Ra_H for moderate values of γ (e.g., $\gamma=0.5$) than for small or large values of γ. A plausible explanation can be made. The flow reversal in the boundary layer due to density inversion is most conspicuous near the

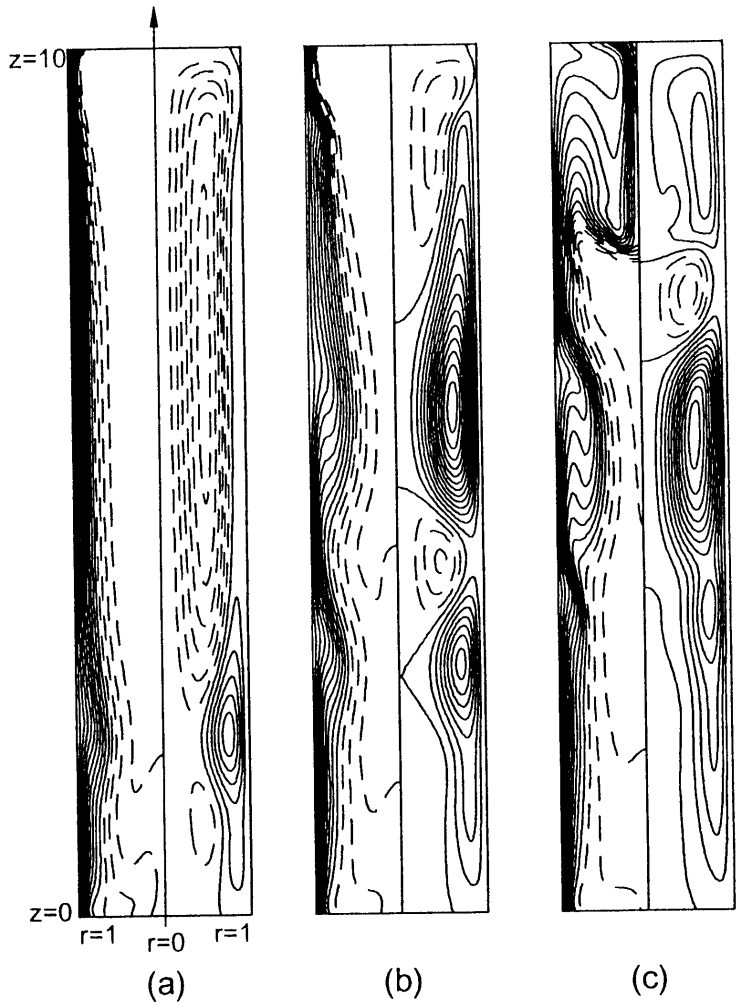

Fig. 9. Same as in Fig. 7, except for $A=10.0$ and $Ra=10^5$. (a) $t=25$; (b) $t=40$; (c) $t=55$. $\Delta\phi=0.005$.

border of flow regime II and III. The boundary layer is prone to instability in the presence of flow reversal in the boundary layer. The velocity shear due to the flow reversal creates an environment for the boundary layer to be unstable so as to generate boundary layer waves. Consequently, owing to the density inversion, the boundary layer instability is seen to occur at a much smaller Ra_H than for a Boussinesq fluid.

7. TRANSIENT PHASES AND TIME SCALES

Time-dependent heat transfer characteristics are described. Fig. 10 depicts the temporal variation of the Nusselt number at the sidewall for the case of $Ra=10^7$, $A=1.0$, and $\gamma=1.0$. The Nusselt number, Nu, is defined as

$$Nu=-\frac{1}{A}\int_0^A \frac{\partial\theta}{\partial r}\Big|_{r=1} dz. \tag{21}$$

Fig. 10 suggests that the full cool-down process can be divided into four distinguishable transient phases. The first, phase I, represents the formation of the sidewall boundary layer. Nu decreases very rapidly with the growth of thermal boundary layer, although the overall value of Nu is very large. In phase II, Nu decreases at a reduced rate. Phase II is associated with the afore-mentioned sidewall

boundary layer restructuring. Phase III corresponds to the transient stage, in which the upper horizontal intrusion and downward propagation of the cold fluid parcels with $\theta < 0$ take place. In this phase, temporal variations of Nu are very small, since the structure of the thermal boundary layer remains virtually unchanged. In the final phase IV, Nu decreases slowly with time, which is closely related to the afore-mentioned decrease in the effective Rayleigh number.

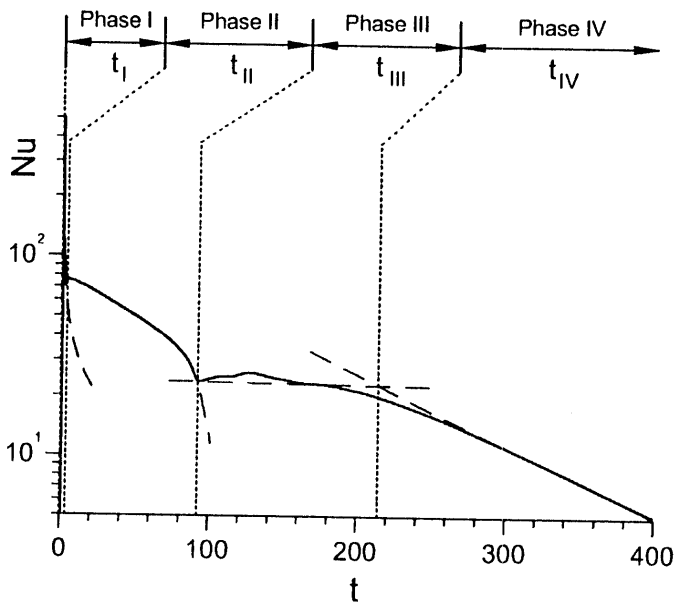

Fig. 10. Phases in the evolution of the Nusselt number. $Ra = 10^7$, $A = 1.0$, and $\gamma = 1.0$.

The effects of γ on the temporal behavior of Nu are illustrated in Fig. 11(a). It is seen that phase II, relating to the boundary layer restructuring, exists only for $\gamma \geq 0.5$, while phases I, III and IV are discernible for all the cases. The time duration for phase II increases with γ. The general transient behavior in phases I, III and IV is similar. The temporal oscillations which are seen in phase III for $\gamma \geq 0.4$ indicate the influences of boundary layer waves. The oscillations of small frequencies are more pronounced for $\gamma = 0.4$ and $\gamma = 0.5$. These are in line with the regime diagram of Fig. 4.

The effect of A on time-dependent heat transfer characteristics is demonstrated in Fig. 11(b). It is notable that the qualitative features of overall transient heat transfer becomes similar if the abscissa is expressed as $t/(RaPr^2A)^{1/4}$. In particular, the effect of A is inconspicuous in phase IV. Fig. 12 illustrates the overall cool-down process by monitoring the time-dependent variations of the mean fluid temperature, $\bar{\theta}$, which is defined as

$$\bar{\theta} = \frac{2}{A} \int_0^A \int_0^1 \theta \, r dr dz. \tag{22}$$

The temporal behavior of $\bar{\theta}$ is generally consistent with the variation of Nu.

Finally, discussions will be focused on the issue of the relevant time scales in cool-down. The characteristic cool-down time scales can be assessed by examining the time durations of the afore-mentioned transient phases. The transition between two successive phases is judged by means of the graphical analysis of the time-dependent Nu curves as shown in Fig. 10. The characteristic curves of four phases are acquired by fitting of the numerical data, and the transition is identified by searching for the intersection point of the curves of two successive phases. The final adjustment process at large times in phase IV becomes diffusive in nature, and it takes place over a long time span. Thus, the time duration for phase IV is estimated up to the time at which $\bar{\theta} = -0.9$, as shown in Fig. 12. Admittedly, a certain amount of arbitrariness is involved in the present classifications of relevant

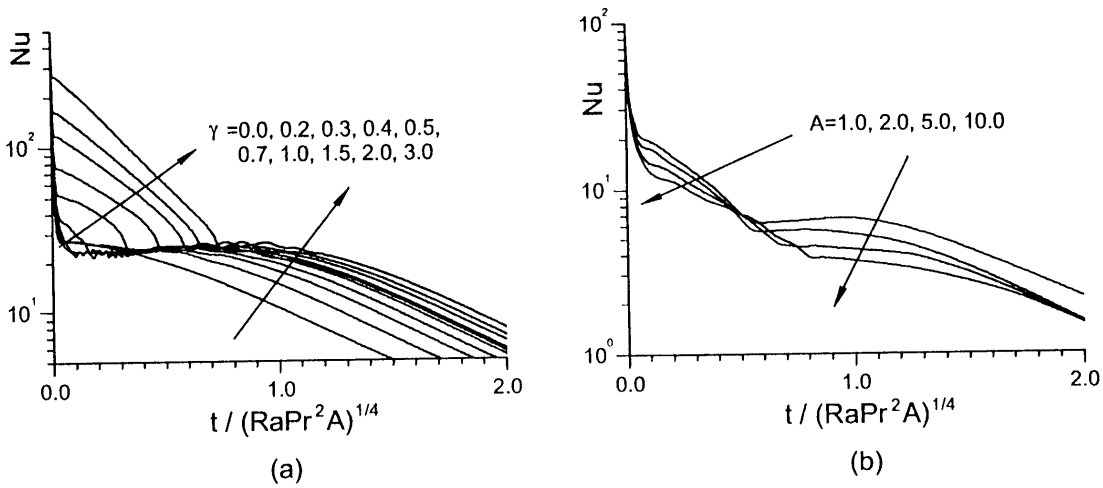

Fig. 11. Effects of γ and A on the evolution of Nu. (a) $Ra=10^7$ and $A=1.0$; (b) $Ra=10^5$, $\gamma=1.0$.

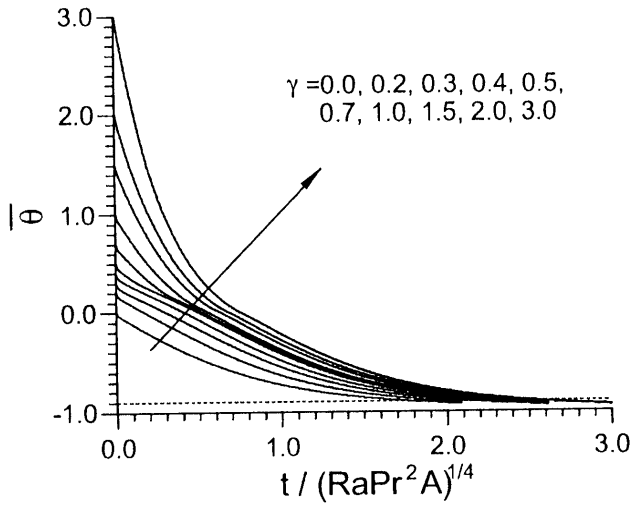

Fig. 12. Temporal variations of the mean fluid temperature. $Ra=10^7$, $A=1.0$, and $\gamma=1.0$.

phases. The main effort is to provide an overall descriptive picture of qualitative essentials of the global cool-down process.

Based on the above method, the time scales of the four transient phases were calculated, which are summarized in Fig. 13. It is clear that t_I increases with γ, and t_I reaches a maximum around at $\gamma=0.4$. For large values of γ, t_I decreases in proportion to $1/\gamma$. The heat transfer rate at the cold wall in the presence of the flow reversal in the vertical boundary layer (for $\gamma=0.3$, 0.4) is smaller than that without the flow reversal ($\gamma\leq 0.2$ and $\gamma\geq 0.5$). Note that δ_T in the former case is also larger than those of latter cases. Consequently, for flow regime II (for $\gamma=0.3$, 0.4), it takes more time for the sidewall boundary layer to grow to its full thickness. However, it is stressed that a precise estimation of t_I is immaterial; the overall magnitude of t_I is much smaller than other time scales (note the difference in units of time in the coordinates of Fig. 13).

The estimated values of t_{II} are plotted in Fig. 13(b). It is immediately clear that t_{II} increases with γ; the effects of Ra and A on t_{II}, scaled by $Ra^{1/4}A^{1/3}$, are minor. Data analysis of the numerical results leads to a correlation

$$t_{II}/(Ra^{1/4}\,Pr^{1/2}\,A^{1/3})=0.5686(\gamma-0.4771)^{0.2996}, \tag{23}$$

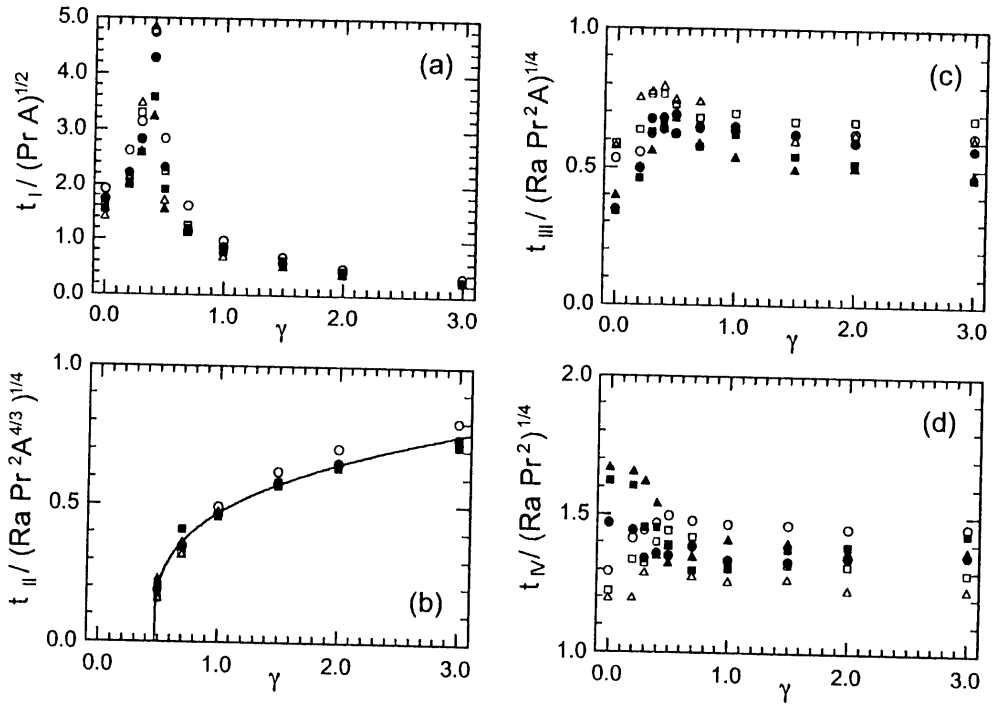

Fig. 13. Scaled time durations for each phase described in Fig. 10. ○, $Ra = 10^5$, $A = 1.0$; □, $Ra = 10^6$, $A = 1.0$; △, $Ra = 10^7$, $A = 1.0$; ●, $Ra = 10^5$, $A = 2.0$; ■, $Ra = 10^5$, $A = 5.0$; ▲, $Ra = 10^5$, $A = 10.0$.

which is shown in the solid-line curve in Fig. 13(b).

Figs. 13(c) and (d) display t_{III} and t_{IV}. The impact of γ on t_{III} and t_{IV} is noticeable only for small values of γ. In particular, t_{III} and t_{IV} are nearly independent of γ for large values of γ. In addition, t_{III} and t_{IV}, scaled by $(RaA)^{1/4}$ and $Ra^{1/4}$ respectively, exhibit only minor dependency on Ra and A. This provides an order-of-magnitude estimation for t_{III} and t_{IV}. The independence of t_{III} and t_{IV} on γ can be explained by the following physical argument. It can be deduced from Fig. 1 and Fig. 6, that the mean temperature falls below 0 in phase III. This implies that the explicit effects of the density inversion decays away in this phase. It is worth recalling that the density inversion effects are represented by the parameter γ. The present Ra is based on the difference between the maximum density and the density at the cold sidewall. Therefore, Ra in the present study is decoupled from the direct effect of density inversion.

By using the definitions of γ and Ra in the present formulation, the effect of γ turns up mostly in the early stages of cool-down when the density inversion is a principal dynamic element. The effects of A becomes insignificant with the progress of cool-down. The parameter Ra becomes the dominant controlling factor in the medium- and large-time adjustment processes when the density inversion effect has subsided.

4. CONCLUSION

The early-time behavior of the boundary-layer flows is controlled largely by the density inversion factor γ. Evolutions of the global fields of velocity and temperature are characterized by Ra and A when γ is very small, and the general features are similar to those of the conventional Boussinesq fluid. The flow reversal in the thermal boundary layer is possible for intermediate values of γ. For large γ, a single cell flow structure is initially developed by the downward flow in the boundary layer. Afterwards, an oppositely-rotating circulation cell emerges from the lower corner region, and the subsequent boundary-layer restructuring along the sidewall is monitored. These are reflective of the

pronounced effects of density inversion in the transient cool-down process. The horizontal intrusion and downward convective filling of cold fluid parcels are seen to follow. Afterwards, slow convective cooling of the fluid is achieved at large times.

The results of the present computations disclose the presence of boundary layer waves traveling along the sidewall. These waves emerge for a large Ra_H, but they are developed at a much smaller Ra_H for moderate values of γ than for a Boussinesq fluid.

The temporal variations of Nu disclose the presence of four distinct phases, which is in line with the description of transient flow and temperature fields. The time durations of the early phases are strongly affected by the strength of density-inversion. The overall times pertinent to the global adjustment process are shown to scale with $Ra^{1/4}$.

REFERENCES

[1] OSTRACH, S.: Natural Convection in Enclosures, *J. Heat Transfer* vol. 110, 1175-1190 (1988).

[2] HYUN, J. M.: Unsteady Buoyant Convection in an Enclosure, *Advances in Heat Transfer* vol. 24, 277-320 (1994).

[3] GEBHART, B. and MOLLENDORF, J. C.: Buoyancy-Induced Flows in Water under Conditions in which Density Extremums May Arise, *J. Fluid Mech.* vol. 89, 673-707 (1978).

[4] VASSEUR, P., ROBILLARD, L. and CHANDRA SHEKAR, B.: Natural Convection Heat Transfer of Water with in a Horizontal Annulus with Density Inversion Effects, *J. Heat Transfer* vol. 105, 117-123 (1983)

[5] INABA, H. and FUKUDA, T.: An Experimental Study of Natural Convection in an Inclined Rectangular Cavity Filled with Water at Its Density Extremum, *J. Heat Transfer* vol. 106, 106-115 (1984).

[6] K. E. LANKFORD and A. BEJAN, A.: Natural Convection in a Vertical Enclosure Filled with Water near 4℃, *J. Heat Transfer* vol. 108, A755-763 (1986).

[7] LIN, D. S. and NANSTEEL, M. W.: Natural Convection Heat Transfer in a Square Enclosure Containing Water near Its Density Maximum, *Int. J. Heat Mass Transfer* vol. 30, 2319-2328 (1987).

[8] LIN, D. S. and NANSTEEL, M. W.: Natural Convection in a Vertical Annulus Containing Water near the Density Maximum, *J. Heat Transfer* vol. 109, 899-905 (1987).

[9] HO, C. J. and LIN, Y. H.: Natural Convection Heat Transfer of Cold Water within an Eccentric Horizontal Cylindrical Annulus, *J. Heat Transfer* vol. 110, 894-900 (1990).

[10] HO, C. J. and LIN, Y. H.: Natural Convection of Cold Water in a Vertical Annulus with Constant Heat Flux on the Inner Wall, *J. Heat Transfer* vol. 112, 117-123 (1990).

[11] ROBILLARD, L. and P. VASSEUR: Convective Response of a Mass of Water near 4℃ to a Constant Cooling Rate Applied on Its Boundaries, *J. Fluid Mech.* vol. 118, 123-141 (1982).

[12] BRAGA B. S. and VISKANTA, R.: Transient Natural Convection of Water near Its Density Extremum in a Rectangular Cavity, *Int. J. Heat Mass Transfer* vol. 35, 861-875 (1992).

[13] MCDONOUGH, M. W. and FAGHRI, A.: Experimental and Numerical Analysis of the Natural Convection of Water through Its Density Maximum in a Rectangular Enclosure, *Int. J. Heat Mass Transfer* vol. 37, 783-801 (1994).

[14] TONG, W. and KOSTER, J. N.: Density Inversion Effect on Transient Natural Convection in a Rectangular Enclosure, *Int. J. Heat Mass Transfer* vol. 37, 927-938 (1994).

[15] VASSEUR, P. and ROBILLARD, L.: Transient Natural Convection Heat Transfer in a Mass of Water Cooled through 4℃, *Int. J. Heat Mass Transfer* vol. 23, 1195-1205 (1980).

[16] ROBILLARD, L. and VASSEUR, P.: Transient Natural Convection Heat Transfer of Water with Maximum Density Effect and Supercooling, *J. Heat Transfer* vol. 103, 528-534 (1981).

[17] DEBLER, W. R.: On the Analogy between Thermal and Rotational Hydrodynamic Stability, *J. Fluid Mech.* vol. 24, 165-176 (1966).

[18] PATANKAR, S. V.: *Numerical Heat Transfer and Fluid Flow.* McGraw-Hill, New York (1980).

[19] HAYASE, T. HUMPHERY, J. A. C. and GRIEF, R.: A Consistently Formulated QUICK Scheme for Fast and Stable Convergence Using Finite-Volume Iterative Calculation Procedures, *J. Comp. Phys.* vol. 98, 108-118 (1992).

[20] PATTERSON J. C. and IMBERGER, J.: Unsteady Natural Convection in a Rectangular Cavity, *J. Fluid Mech.* vol. 100, 65-86 (1980).

[21] EL-HENAWY, I., GEBHART, B., HASSARD, B., KAZARINOFF, N. D. and MOLLENDORF, J. C.: Numerically Computed Multiple Steady States of Vertical Buoyancy-Induced Flows in Cold Pure Water. *J. Fluid Mech.* 122, 235-250 (1982).

[22] HWANG, Y., KAZARINOFF, N. D. and MOLLENDORF, J. C.: Hydrodynamic Stability of Multiple Steady-States of Vertical Buoyancy-Induced Flows in Cold Pure Water, *Int. J. Heat Mass Transfer* vol. 36, 423-435 (1993).

[23] PAOLUCCI, S. and CHENOWETH, D. R.: Transition to Chaos in a Differentially Heated Vertical Cavity, *J. Fluid Mech.* vol. 201, 370-410 (1989).

[24] LE QUE'RE', P.: Transition to Unsteady Natural Convection in a Tall Water-Filled Cavity, *Phys. Fluids A* vol. 2, 503-514 (1990).